Synthesis and Magnetic Properties of New $[Fe_{18}S_{25}](TETAH)_{14}$ (TETAH = Protonated Triethylenetetramine) Nanoribbons: An Efficient Precursor to Fe_7S_8 Nanowires and Porous Fe_2O_3 Nanorods

Zheng-An Zang, Hong-Bin Yao, Yu-Xue Zhou, Wei-Tang Yao, and Shu-Hong Yu*

Division of Nanomaterials & Chemistry, Hefei National Laboratory for Physical Sciences at Microscale, the School of Chemistry and Materials, University of Science and Technology of China, Hefei, 230026, P.R. China

Received March 26, 2008. Revised Manuscript Received May 21, 2008

A solvothermal reaction in a mixed solvent made of triethylenetetriamine (TETA) and deionized water (DIW) results in the formation of well-defined $[Fe_{18}S_{25}](TETAH)_{14}$ nanoribbons. A suitable volume ratio of TETA and DIW is essential for the formation of elegant $[Fe_{18}S_{25}](TETAH)_{14}$ nanoribbons. The $[Fe_{18}S_{25}](TETAH)_{14}$ nanoribbons can act as efficient precursors for production of either Fe_7S_8 nanowires or porous α-Fe_2O_3 nanorods by thermal decomposition of $[Fe_{18}S_{25}](TETAH)_{14}$ in an argon or air atmosphere. The present study demonstrates that the combination of small molecule polyamine with magnetic semiconductor makes it possible to obtain new hybrid nanostructured materials. The thermal decomposition of this new hybrid material is a powerful tool as a unique pathway for controlled synthesis of transition metal chacolgenide nanomaterials and porous transition metal oxides.

1. Introduction

Inorganic−organic hybrid materials have been intensively studied, not only for their tremendous potential in providing enhanced material properties that are not easily achievable with either organic or inorganic materials alone but also for their many technological applications.[1] A new family of II−VI based ordered hybrid semiconductors can be synthesized by incorporating segments (e.g., slab, chain) of a II−VI semiconductor MQ and organic spacers (L) in one structure via coordinate or covalent bonds.[2] While possessing uniform and periodic crystal structures, the resultant three-dimensional networks $[MQ(L)_{0.5}]$ (M = Mn, Zn, Cd; Q = S, Se, Te; L = diamine, deta) exhibit a very large blue shift in their optical adsorption edge due to a strong quantum confinement effect (QCE) induced by the internal subnanostructures.[2–4] Recently, our group introduced solvothermal methodologies into the syntheses of flexible ZnS nanobelts[5] and inorganic−organic hybrid $[ZnSe](DETA)_{0.5}$ nanobelts.[6] However, low-dimensional transition metal chalcogenide semiconductors based on hybrid nanomaterials have rarely been reported.[7] Rational design and synthesis of hybrid transition metal chalcogenide nanocomposites with interesting properties remains a challenging endeavor.

On the other hand, magnetic nanomaterials have attracted a tremendous amount of attention from researchers in various disciplines due to their fundamental and technological applications, including magnetic storage media, ferrofluids, contrast agents for magnetic resonance imaging, and magnetic carriers for drug targeting.[8] Iron sulfide, as an important magnetic material among other transition metal chalcogeides, has drawn considerable attention and has been extensively studied for many years. For example, iron disulfide (pyrite, FeS_2) is a very important material for producing polycrystalline solar cells.[9] However, only a few one-dimensional nanostructured iron sulfides have been reported so far, such as FeS_2 nanorods prepared by a solvothermal process.[10] Iron sulfide nanowires such as Fe_7S_8 and $Fe_{1-x}S$ were synthesized by thermal decomposition of $Fe_{1-x}S(en)_{0.5}$ nanowires, which were obtained by a solvothermal method in ethylenediamine

* To whom correspondence should be addressed. Fax: + 86 551 3603040. E-mail:shyu@ustc.edu.cn.

(1) (a) Mitzi, D. B. In *Progress in Inorganic Chemistry*; Karlin, K. D. , Ed.; Wiley: New York, 1999; p 1. (b) Ishihara, T. In *Optical Properties of Low-Dimensional Materials*; Ogawa, T., Kanemitsu, Y., Eds.; World Scientific: Singapore, 1995; p 289.
(2) (a) Huang, X. Y.; Li, J.; Fu, H. X. *J. Am. Chem. Soc.* **2000**, *122*, 8789. (b) Heulings, H. R.; Huang, X. Y.; Li, J.; Yuen, T.; Lin, C. L. *Nano Lett.* **2001**, *1*, 521. (c) Huang, X. Y.; Heulings, H. R.; Le, V.; Li, J. *Chem. Mater.* **2001**, *13*, 3754. (d) Huang, X. Y.; Li, J.; Zhang, Y.; Mascarenhas, A. *J. Am. Chem. Soc.* **2003**, *125*, 7049.
(3) Yu, S. H.; Yoshimura, M. *Adv. Mater.* **2002**, *14*, 296.
(4) (a) Deng, Z. X.; Wang, C.; Sun, X. M.; Li, Y. D. *Inorg. Chem.* **2002**, *41*, 869. (b) Deng, Z. X.; Li, L. B.; Li, Y. D. *Inorg. Chem.* **2003**, *42*, 2331.
(5) Yao, W. T.; Yu, S. H.; Pan, L.; Li, J.; Wu, Q. S.; Zhang, L.; Jiang, J. *Small* **2005**, *1*, 320.
(6) Yao, W. T.; Yu, S. H.; Huang, X. Y.; Jiang, J.; Zhao, L. Q.; Pan, L.; Li, J. *Adv. Mater.* **2005**, *17*, 2799.
(7) Nath, M.; Choudhury, A.; Rao, C. N. R. *Chem. Commun.* **2004**, 2698.
(8) (a) Schmid, G. *Nanoparticles: From Theory to Application*; Wiley-VCH: Weinheim, 2004. (b) Klabunde, K. J. *Nanoscale Materials in Chemistry*; Wiley-Interscience: New York, 2001. (c) Fendler, J. H. *Nanoparticles and Nanostructured Films*; Wiley-VCH: Weinheim, 1998. (d) Fertman, V. E. *Magnetic Fluids Guide Book: Properties and Applications*; Hemisphere Publishing Co.: New York, 1990. (e) Berkovsky, B. M.; Medvedev, V. F.; Krakov, M. S. *Magnetic Fluids: Engineering Applications*; Oxford University Press: Oxford, 1993. (f) Hyeon, T. *Chem. Commun.* **2003**, 927. (g) Zhang, J. Z.; Wang, Z. L.; Liu, J.; Chen, S.; Liu, G.-Y. *Self-Assembled Nanostructures*; Kluwer Academic/Plenum Publishers: New York, 2003.
(9) (a) Ennaoui, A.; Tributsch, H. *Sol. Cells* **1984**, *13*, 197. (b) Ennaoui, A.; Fiechter, S.; Tributsch, H. *J. Electrochem. Soc.* **1985**, *132*, 1579. (c) Ennaoui, A.; Fiechter, S.; Jaegermann, W.; Tributsch, H. *J. Electrochem. Soc.* **1986**, *133*, 97.
(10) Qian, X. F.; Xie, Y.; Qian, Y. T. *Mater. Lett.* **2001**, *48*, 109.

10.1021/cm800871f CCC: $40.75
Published on Web 06/27/2008

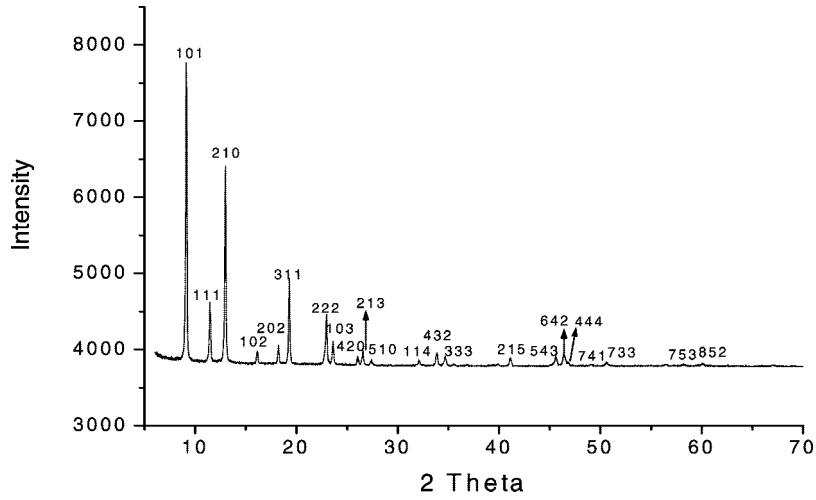

Figure 1. PXRD pattern of the hybrid $[Fe_{18}S_{25}](TETAH)_{14}$ indexed by Powder X.

(en) media.[11] Both greigite and marcasite are metastable,[12] and their instability was also reported in solvothermal synthesis.[13,14] Pyrite (FeS_2) nanowires, nanoribbons, and nanotubes[15] have also been synthesized in ethylenediamine due to their chelating property.[16] FeS_2 semiconductor monocrystalline 2D nanowebs were prepared by using a hyposulfite self-decomposition route.[17] Recently, our group successfully developed a magnetic-field-induced phase-selective synthesis of ferrosulfide microrods by a hydrothermal process using amino acid as a crystal growth modifier.[18]

In this paper, $[Fe_{18}S_{25}](TETAH)_{14}$ (TETA: triethylenetetramine) nanoribbons with a width of 100−250 nm, a thickness of 10−30 nm, and a length up to 10 μm have been synthesized by a mixed solvent strategy using $FeSO_4 \cdot 7H_2O$ and C_2H_5NS as reactants. The volume ratio of triethylenetetramine (TETA) and deionized water (DIW) has significant influence on the morphology of the product. Thermal decomposition of$[Fe_{18}S_{25}](TETAH)_{14}$ nanoribbons resulted in the formation of Fe_7S_8 nanowires and porous Fe_2O_3 rods. The magnetic properties of the $[Fe_{18}S_{25}](TETAH)_{14}$ nanoribbons and Fe_7S_8nanowires are also studied.

2. Experimental Section

Synthesis of $[Fe_{18}S_{25}](TETAH)_{14}$. All chemicals are analytical grade and used as received without further purification. In a typical procedure, $FeSO_4 \cdot 7H_2O$ (1 mmol) and thioacetamide (C_2H_5NS, 2 mmol) were added to a mixed solvent of TETA and DIW (total 18 mL, V_{TETA}:V_{DIW} = 1:2) with stirring. The mixed solution was then transferred into a Teflon-lined autoclave (with a filling ratio of 80%).

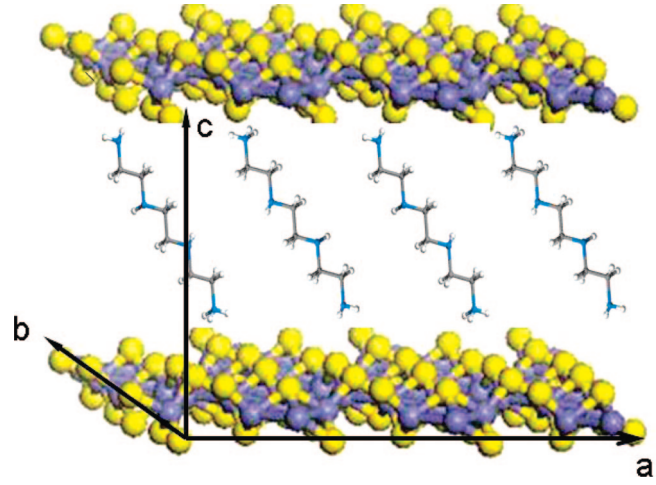

Figure 2. Proposed structure of $[Fe_{18}S_{25}](TETAH)_{14}$. The yellow balls are sulfur; dark purple balls, Fe; blue balls, N; gray balls, C; white balls, H.

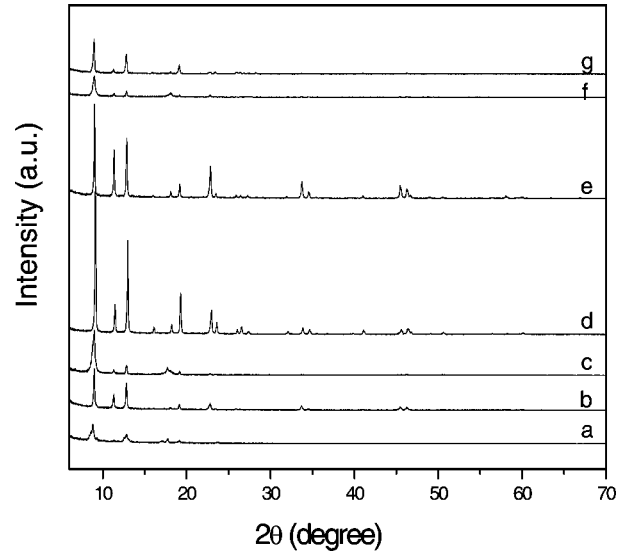

Figure 3. PXRD patterns of the products prepared in a mixed solvent with different ratios of V_{TETA}:V_{DIW} at 140 °C for 24 h. (a) Prepared in pure TETA; (b) 6:1; (c) 3:1; (d) 1:1; (e) 1:2; (f) 1:3; (g) 1:6.

The autoclave was closed and heated in an oven at 140 °C for 24 h before it was cooled to room temperature naturally. The black

(11) Nath, M.; Choudhury, A.; Kundu, A.; Rao, C. N. R. *Adv. Mater.* **2003**, *15*, 2098.
(12) Vaughan, D. J.; Lennie, A. R. *Sci. Prog.* **1991**, *75*, 371.
(13) Qian, X. F.; Zhang, X. M.; Wang, C.; Xie, Y.; Wang, Z.; Qian, Y. T. *Mater. Sci. Eng., B* **1999**, *64*, 170.
(14) Chen, X. Y.; Zhang, X. F.; Wan, J. X.; Wang, Z. H.; Qian, Y. T. *Chem. Phys. Lett.* **2005**, *403*, 396.
(15) (a) Kar, S.; Chaudhuri, S. *Chem. Phys. Lett.* **2004**, *398*, 22. (b) Kar, S.; Chaudhuri, S. *Mater. Lett.* **2005**, *59*, 289.
(16) Yu, S. H.; Yang, J.; Han, Z. H.; Zhou, Y.; Yang, R. Y.; Qian, Y. T.; Zhang, Y. H. *J. Mater. Chem.* **1999**, *9*, 1283.
(17) Gao, P.; Xie, Y.; Ye, L. N.; Chen, Y.; Guo, Q. X. *Cryst. Growth Des.* **2006**, *6*, 583.
(18) He, Z. B.; Yu, S. H.; Zhou, X. Y.; Li, X. G.; Qu, J. F. *Adv. Funct. Mater.* **2006**, *16*, 1105.

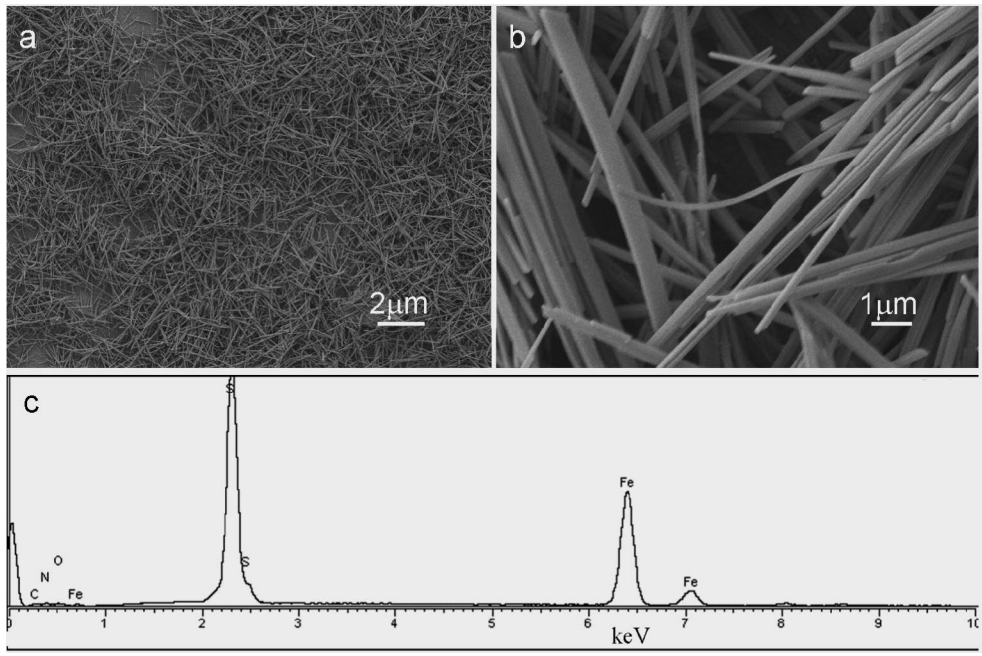

Figure 4. (a, b) SEM images of $[Fe_{18}S_{25}](TETAH)_{14}$ nanoribbons prepared in a mixed solvent (the volume ratio of V_{TETA}:V_{DIW} = 1:2). (c) Energy-dispersive spectrum of $[Fe_{18}S_{25}](TETAH)_{14}$.

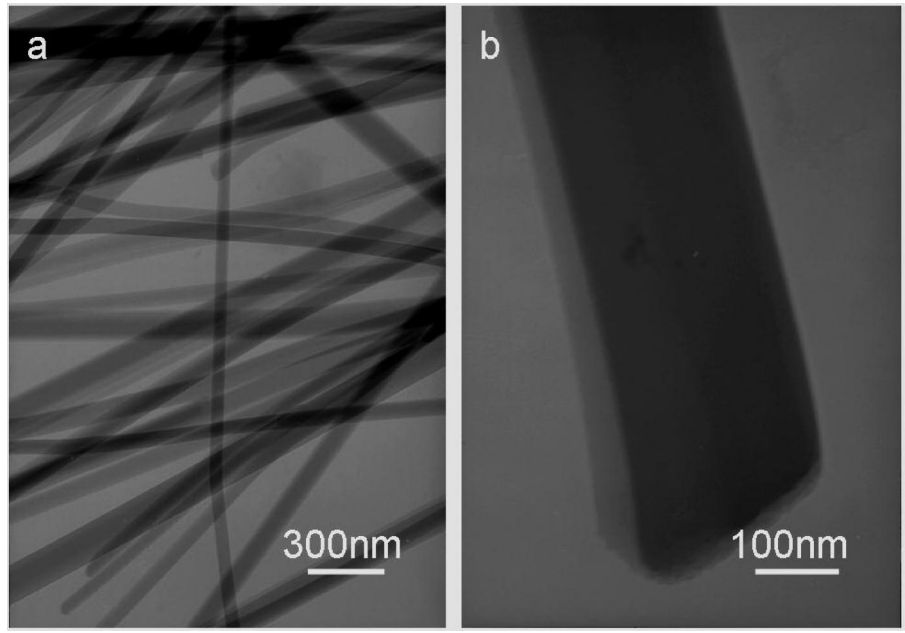

Figure 5. TEM images of $[Fe_{18}S_{25}](TETAH)_{14}$ nanoribbons prepared in a mixed solvent with a volume ratio of V_{TETA}:V_{DIW} = 1:2. (a) A general overview and (b) a typical nanoribbon.

floccule formed after the reaction was washed by distilled water and absolute ethanol, respectively, and dried in a vacuum oven at 80 °C for 6 h. The thermal decomposition of the $[Fe_{18}S_{25}](TETAH)_{14}$ precursor for producing Fe_7S_8 nanowires and porous Fe_2O_3 rods was performed in a furnace with temperature and carrying gas controller under N_2 and air atmosphere, respectively.

Characterization. Powder X-ray diffraction patterns (PXRD) of the products were run on a Japan Rigaku DMax-γA rotation anode X-ray diffractometer equipped with graphite monochromatized Cu Kα radiation (λ = 1.54178 Å). Transmission electron microscope (TEM) photographs were taken on an Hitachi Model H-800 transmission electron microscope at an accelerating voltage of 200 kV. The morphologies and sizes of the samples were examined by field emission scanning electron microscopy (FESEM, JEOL JSM-6700F, operated at 10 kV). Element analysis was conducted by energy-dispersive spectra (EDS) on a JEOL JSM 6700 scanning electron microanalyzer (SEM).The infrared spectra were obtained on a Fourier transform infrared spectrometer (FTIR,Magna-IR-750); thermogravimetric analysis (TGA) was carried out on a TGA-50 thermal analyzer (Shimadzu Corporation) with a heating rate of 10 °C min^{-1} in flowing nitrogen. The magnetic measurements on powdered samples in a medical cap were carried out at 4 K using a commercial SQUID magnetometer (MPMS-XL) from Quantum Design Corp.

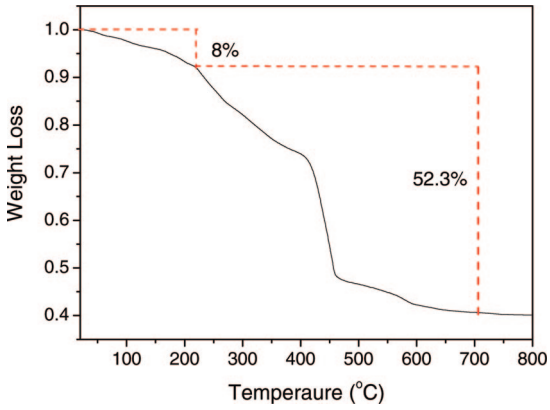

Figure 6. Thermogravimetric analysis curve of the $[Fe_{18}S_{25}](TETAH)_{14}$ nanoribbons prepared at 140 °C for 24 h, V_{TETA}:V_{DIW} = 1:2. TGA measurement was run under N_2 flow.

3. Results and Discussion

Synthesis of $[Fe_{18}S_{25}](TETAH)_{14}$ and Structure Analysis. This hybrid material is one new kind of material. The small-angle PXRD has been run on the hybrid material (see Supporting Information Figure S1). No strong peak appears at very low 2θ angles (<5°). Thus, this hybrid material is not isostructural to $ZnSe(deta)_{0.5}$ as reported previously.[2,6]Furthermore, it is difficult to grow a large enough single crystal for this hybrid material, possibly due to the TETA molecule used in this system. In this case, we could propose only the potential formula of this hybrid and structure based on the elemental analysis and modeling PXRD indexing results. The elemental analysis data (see Supporting Information Table S1) indicates the element molar ratio Fe:S:N:C = 0.72:1:1.96:2.91, partly detailed N:C = 1:1.48 and the calculation of N:C in TETA is 1:1.5. On the other hand, the PXRD was indexed by the TEROR method using program Powder X.[19] The indexed results (Supporting Information Table S2 and Figure 1) show that the space group is P_6C/mm and the unit cell is $a = b =$ 20.96 Å, c = 11.60 Å. With the combination of the unit cell size, atoms, and molecule ratio and electrical neutrality principles, the possible formula of this hybrid material is determined as $[Fe_{18}S_{25}](TETAH)_{14}$. Based on the proposed formula, we suppose that the structure of this hybrid is composed of $[Fe_{18}S_{25}]^{14-}$ layers and TETAH molecules inserted between the layers, and specifically the $[Fe_{18}S_{25}]^{14-}$ layer is along the *ab* plane and TETAH is along the *c* axis as illustrated in Figure 2.

Morphology Control Synthesis of $[Fe_{18}S_{25}](TETAH)_{14}$ Nanoribbons. The reaction occurred in pure TETA, as well as in other mixed solvents with different volume ratios of TETA and DIW, and resulted in the formation of hybrid material $[Fe_{18}S_{25}](TETAH)_{14}$ as confirmed by the PXRD pattern in Figure 3a−f. Although the phase remained unchanged for the products obtained in mixed solvents with different volume ratios, the morphologies of $[Fe_{18}S_{25}](TETAH)_{14}$ product are different. When the volume ratio of TETA and DIW reached up to 1:2, uniform and elegant $[Fe_{18}S_{25}](TETAH)_{14}$ nanoribbons can be obtained as shown in (Figures 4 and 5).

The influence of the volume ratio of TETA and DIW on the formation of $[Fe_{18}S_{25}](TETAH)_{14}$ nanostructures has also been investigated. When the volume of TETA was dominant, the morphology of the products tended to be a mixture of wires and a few microparticles (Supporting Information Figure S1a−c). For example, a mixture of microbelts and microparticles was produced when the volume ratio of TETA and DIW reached up to 6:1. However, when the ratio of V_{TETA}:V_{DIW} decreased to 1:2 and 1:3, respectively, short nanorods and relative uniform nanowires formed (Figure 4, and Supporting Information Figure S1e). Field emission scanning electron micrographs (FE-SEM) show that the length of the hybrid ribbons can reach up to several tens of micrometers (Figure 4a,b). TEM images show that the hybrid ribbons have widths in the range of 100−250 nm and thickness of about 80 nm (Figure 5a,b).

In the FT-IR spectra of the product, the vibration bands of $-CH_2$ from the TETA molecule can be observed (Supporting Information Figure S2), which implies the existence of TETA in the product. Compared with the IR spectrum of pure TETA, the vibration band of $-NH_2$ at 1600 cm^{-1} shifts to a lower wavenumber (1585 cm^{-1}) in the spectrum of $[Fe_{18}S_{25}](TETAH)_{14}$ due to the protonation of TETA.

Conversion of $[Fe_{18}S_{25}](TETAH)_{14}$ Nanoribbons to Fe_7S_8 Nanowires and Porous α-Fe_2O_3 Nanorods. The thermogravimetric anlaysis (TGA) of the product shows two steps of weight loss: The first step is up to 220 °C and a slight weight loss is about 8 wt %), which is mainly due to the loss of the adsorbed water and possibly free TETA adsorbed on the surface of the ribbons. The second step is up to 700 °C and shows the net weight loss is about 52.3 wt % due to the loss of the protonated triethylenetetriamine and sufficient sulfur in the hybrid material (Figure 6), which is consistent with the calculated result (52.6wt%) based on the conversion from $[Fe_{18}S_{25}](TETAH)_{14}$ to Fe_7S_8 (JCPDS 25-0411). Thermal decomposition of this hybrid at 800 °C in an Ar atmosphere for 4−6 h results in the formation of pure Fe_7S_8 inorganic phase, which is confirmed by the PXRD pattern (Supporting Information Figure S3).

The FE-SEM images show that Fe_7S_8 nanowires with coarse surfaces are produced (Figure 7a,b) and the rough surface is caused by elimination of TETAH from hybrid $[Fe_{18}S_{25}](TETAH)_{14}$ nanoribbons. If this hybrid is exposed to air for heat treatment, the PXRD of the as-obtained brick red product is in good agreement with α-Fe_2O_3 phase (Supporting Information Figure S4, JCPDS 86-0550). The FE-SEM images and TEM images of the heat-treated product in air also display porous nanostructures (Figures 8 and 9). Hence, iron sulfides and iron oxides can be easily obtained from the same precursor through a simple thermal decomposition procedure as illustrated in Scheme 1.

The porosity of the α-Fe_2O_3 nanorods produced by thermal decomposition of $[Fe_{18}S_{25}](TETAH)_{14}$ nanoribbons in air was determined by N_2 adsorption by BET (Brunauer−Emmett−Teller) measurements using an ASAP-2000 surface area analyzer. N_2 adsorption−desorption isotherm and the pore size distribution cure for the porous α-Fe_2O_3 are shown in Figure

(19) Dong, C *J. Appl. Crystallogr.* **1999**, *32*, 838. (PowderX: Windows-95 based program for powder X-ray diffraction data processing.)

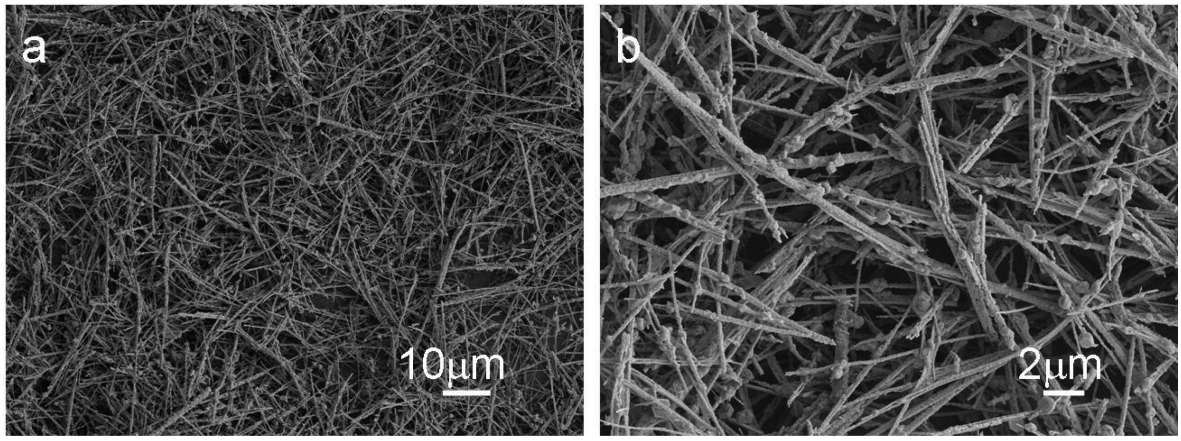

Figure 7. (a, b) Low- and high-magnification FE-SEM images of Fe_7S_8 nanowires produced by thermal decomposition of $[Fe_{18}S_{25}](TETAH)_{14}$ nanoribbons in Ar atmosphere.

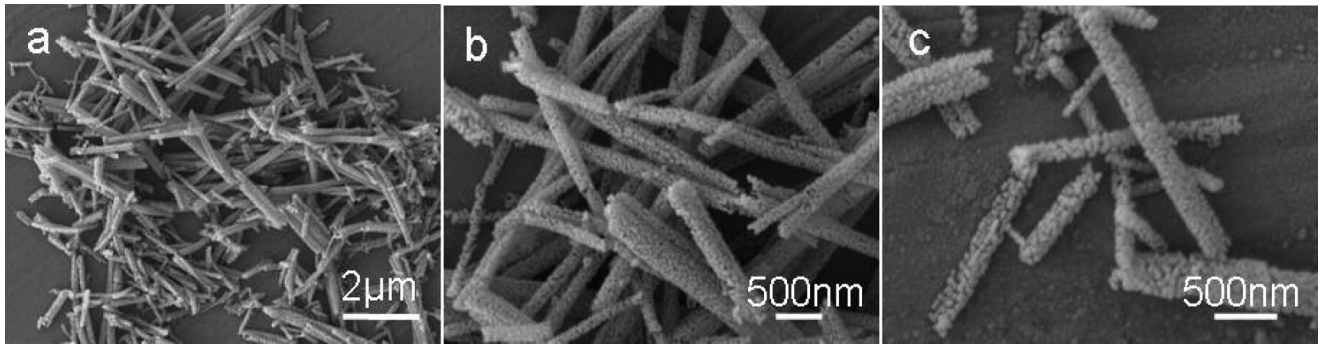

Figure 8. (a, b) Low- and high-magnification FE-SEM images of α-Fe_2O_3 products obtained by thermal decomposition of $[Fe_{18}S_{25}](TETAH)_{14}$ nanoribbons at 600 °C for 1 h in air atmosphere.

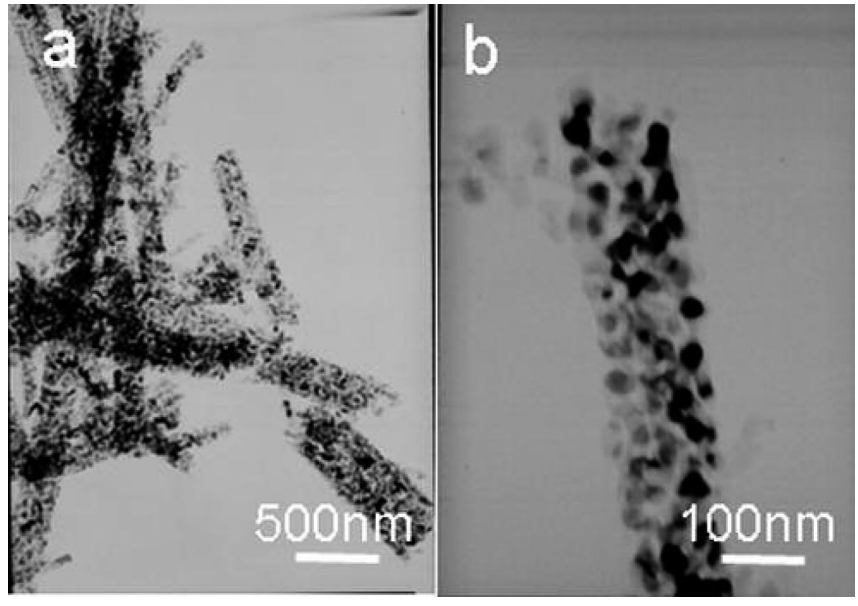

Figure 9. (a, b) TEM images of α-Fe_2O_3 product obtained by thermal decomposition of $[Fe_{18}S_{25}](TETAH)_{14}$ nanoribbons in air atmosphere.

10, which indicates that there are nanospores in the α-Fe_2O_3 nanorods. The BET (Brunauer−Emmett−Teller) surface area is about 23.65 m^2/g and the BJH (Barret−Joyner−Halenda) average pore diameter is about 65 nm. The data implies that the porous α-Fe_2O_3 as obtained could be potentially applied in adsorption and various catalytic reactions, as in the removal of heavy metal ions and other pollutants in water treatment.[20]

Magnetic Properties of $[Fe_{18}S_{25}](TETAH)_{14}$ Nanoribbons and Fe_7S_8 Nanowires. The magnetic properties of the $[Fe_{18}S_{25}](TETAH)_{14}$ and thermal decomposition product Fe_7S_8 nanowires have been investigated. The superparamagnetic relaxation of $[Fe_{18}S_{25}](TETAH)_{14}$ nanoribbons

(20) Zhong, L. S.; Hu, J. S.; Liang, H. P.; Cao, A. M.; Song, W. G.; Wan, L. J. *Adv. Mater.* **2006**, *18*, 2426.

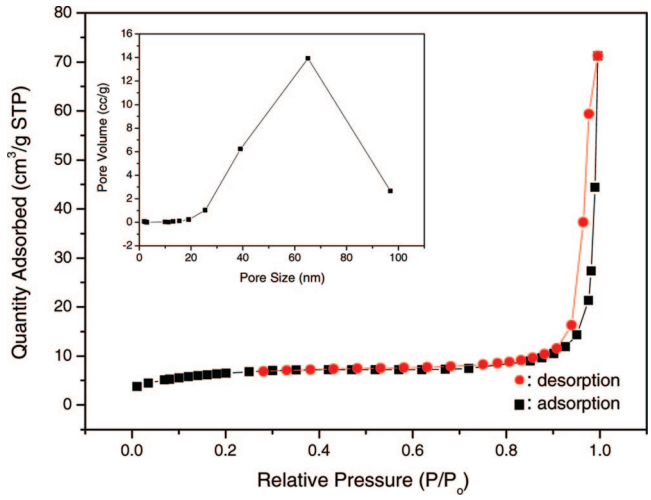

Figure 10. N_2 adsorption−desorption isotherm curve and pore size distribution (insert) of porous α-Fe_2O_3.

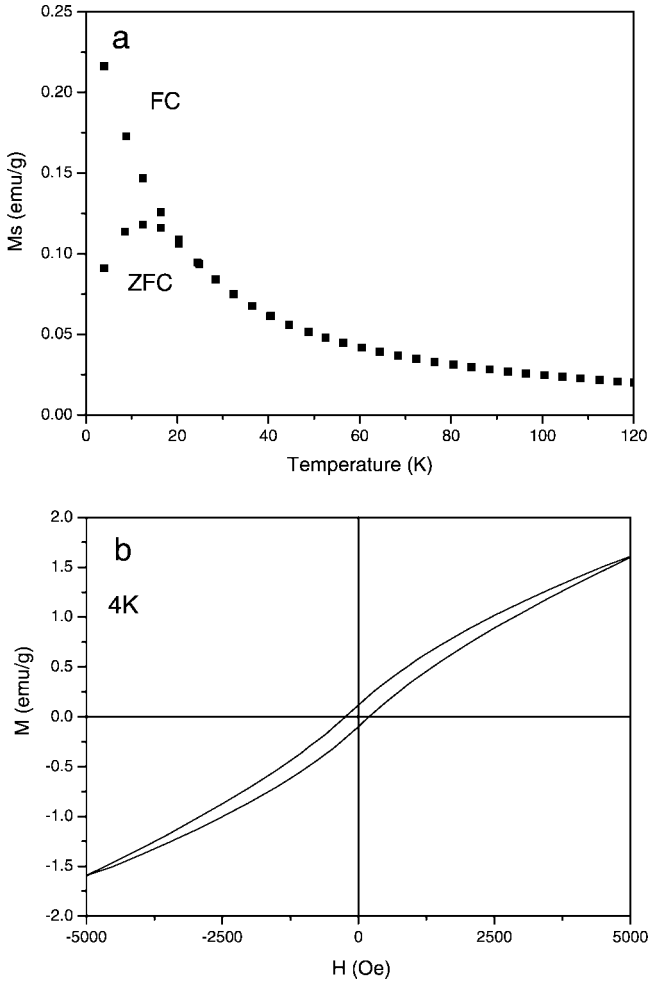

Figure 11. (a) *M*(*T*) curves under 120 Oes (FC and ZFC represent field-cooling and zero-field-cooling, respectively); (b) the hysteresis loop curve of $[Fe_{18}S_{25}](TETAH)_{14}$ nanoribbons.

is studied by field-cooled (FC) and zero-field-cooled (ZFC) magnetization. FC and ZFC magnetization measurements are performed at 200 G (Figure 11a). The divergence of the FC and ZFC data below $T_c = 20$ K indicates the formation of an ordered magnetic state. The blocking temperature (T_b) is

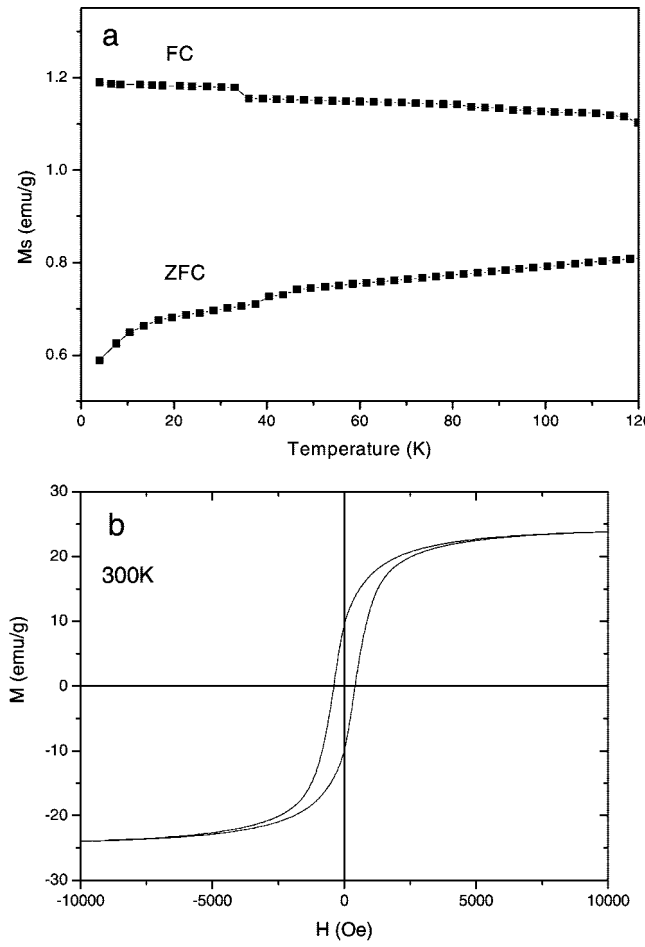

Figure 12. (a) *M*(*T*) curves under 120 Oes (FC and ZFC represent field-cooling and zero-field-cooling, respectively); (b) the hysteresis loop curve of Fe_7S_8 nanowires.

Scheme 1. Schematic Illustration of the Formation of Fe_7S_8 and α-Fe_2O_3 by Thermal Decomposition of $[Fe_{18}S_{25}](TETAH)_{14}$ Nanoribbons under Different Atmospheres

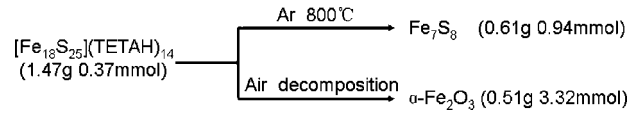

12.5 K, below which the superparamagnetic transition is blocked. Furthermore, a hysteresis loop has been observed at 4 K with a coercive field (H_c) of 300 Oe (Figure 11 b).

Figure 12a shows the magnetization vs temperature plot of Fe_7S_8 nanowires. It is clear that the diversity of FC and ZFC at the same temperature is much higher than that of $[Fe_{18}S_{25}](TETAH)_{14}$ nanoribbons, which indicates a much stronger magnetic coupling between magnetic moments in Fe_7S_8 as a result of the TETAH elimination from the interlayer structures. Figure 12b shows the hysteresis plot for Fe_7S_8 nanowires at room temperature, indicating that both the saturation magnetization and the coercive field of Fe_7S_8 rods are much higher than those of $[Fe_{18}S_{25}](TETAH)_{14}$ nanowires even at room temperature.

Based on the magnetic comparison between $[Fe_{18}S_{25}](TETAH)_{14}$ and Fe_7S_8, it is obvious that organic amine molecule can affect the magnetic properties of the Fe−S system, even change it from ferromagnetic to super-

paramagnetic performance. This phenomenon offers some evidence that magnetic properties of a ferromagnetic material can be changed by intercalating organic amine molecules. In addition, it could be predicted that the magnetic performance of the hybrid material could be tuned by introducing different organic amine molecules, which is worth further investigation in future.

4. Conclusions

In summary, well-defined $[Fe_{18}S_{25}](TETAH)_{14}$ nanoribbons have been synthesized successfully by using a binary mixed solvent composed of triethylenetetriamine (TETA) and deionized water (DIW). A suitable volume ratio of TETA and DIW is essential for the formation of elegant $[Fe_{18}S_{25}](TETAH)_{14}$ nanoribbons. The FC (field-cooled) and ZFC (zero-field-cooled) magnetization measurements of the $[Fe_{18}S_{25}](TETAH)_{14}$ nanoribbons performed at 200 G show the divergence of the FC and ZFC data below $T_c = 20$ K because of the formation of an ordered magnetic state. A hysteresis loop has been observed at 4 K with a coercive field (H_c) of 300 Oe. In addition, the $[Fe_{18}S_{25}](TETAH)_{14}$ nanoribbons can act as efficient precursors for production of either Fe_7S_8 nanowires or porous α-Fe_2O_3 nanorods by thermal decomposition in argon or air atmosphere. The present study demonstrates that the combination of small molecule polyamine with magnetic semiconductor makes it possible to obtain new hybrid nanostructure materials, which could act as unique precursors for templating synthesis of a variety of transition meal chalcogenides or metal oxides.

Acknowledgment. This work is supported by the National Science Foundation of China (NSFC) (Grants 50732006, 20621061,20671085,20701035,20325104,50372065),2005CB623601, the special funding support from the Centurial Program of Chinese Academy of Sciences, Anhui Development Fund for Talent Personnel and Anhui Education Committee (2006Z027, ZD2007004-1), the Specialized Research Fund for the Doctoral Program (SRFDP) of Higher Education State Education Ministry, and the Partner-Group of the Chinese Academy of Sciences-the Max Planck Society.

Supporting Information Available: Additional figures and tables (PDF). This material is available free of charge via the Internet at http://pubs.acs.org.

CM800871F